TREND

Trapped Radiation Environment Model Development

Technical Note 6 Part II

Improvement of the Trapped Proton Anisotropy Description

ESTEC Contract No. 10725/94/NL/JG(SC)*

M. Kruglanski (IASB)

D. Heynderickx (BIRA)

August 1998

*ESA Technical Management: E.J. Daly (WMA)

Contents

Foreword **v**

Introduction **1**

4 Generalised anisotropy model **3**
4.1 Magnetic drift shell parameters 3
4.2 Finite gyroradius effect 5
4.3 First order expansion of the perpendicular flux 6
4.4 Natural coordinate system 7
4.5 Evaluation of ΔL 9
4.6 Comments 11

5 Comparison with observational data **13**
5.1 Variation of L_{GC} 16
5.2 Flux scale height 17
5.3 East-West asymmetry 19
5.4 Comparison with previous models 21
5.4.1 Watts et al. (1989) model 23
5.4.2 BK-MIN model 24
5.4.3 New semi-empirical model 24
5.4.4 Comparison 27

References **29**

List of Figures

4.1 Representation of three consecutive magnetic drift shell 7
4.2 Representation of a helicoidal trajectory 8

5.1 SAMPEX 86–120 MeV proton countrate as a function of L and B_{m} 14
5.2 Representation of the magnetic drift shell $L = 1.24$, $B_{\mathrm{m}} = 0.2$ 15
5.3 Geocentric altitude of the southern mirror points of the drift shell ($L = 1.24$, $B_{\mathrm{m}} = 0.2$) 16
5.4 The variation ΔL of the shell parameter as a function of the azimuthal angle β 17
5.5 The SAMPEX 86–120 MeV proton countrate as a function of the shell parameter L 18
5.6 The SAMPEX 86–120 MeV proton countrate as a function of L_{GC} . 19
5.7 The SAMPEX 86–120 MeV proton countrate as a function of the azimuthal angle β 20
5.8 Representation of the coordinate system used to compare different proton anisotropy models 21
5.9 Comparison of the Heckman & Nakano (1969) and Badhwar & Konradi (1990) pitch angle distributions 22
5.10 Dependence of the directional 100-MeV proton flux on the polar and azimuthal direction at the position (394.3 km, 25.7°S, 51.0°W) . . . 25
5.11 Dependence of the directional 100-MeV proton flux on the polar and azimuthal direction at the position (720.8 km, 7.9°S, 15.0°W) 26

Foreword

This Technical Note is the second part of Technical Note 6, *Trapped Proton Anisotropy at Low Altitudes*. Both parts of Technical Note 6 have been prepared in fullfilment of the Workpackages WP.2.2 and WP.2.3R of the TREND-3 study related to *Radiation Environments of Astronomy Missions and LEO Missions*. The TREND-3 study was financed by ESA/ESTEC TRP Contracts No. 7917/93/NL/JG and No. 10725/94/NL/JG(SC).

We would like to thank J.B. Blake and M. Looper and of Aerospace Corp. for providing us with the SAMPEX/PET proton flux data.

Introduction

At the inner edge of the radiation belts, the trapped proton fluxes are highly anisotropic due to the interaction of the particles with the Earth's atmosphere. An important part of the flux anisotropy consists of a steep pitch-angle distribution related to the atmospheric loss cone. An additional azimuthal anisotropy appears for the high-energy trapped proton fluxes. This anisotropy is observable when the scale length of the proton fluxes is comparable to or shorter than the size of the proton gyration radius. The azimuthal anisotropy results in an East-West asymmetry effect where the fluxes of protons coming—for a given position—from the East are higher than the fluxes of proton coming from the West. Generally, for spacecraft shielding calculations, omnidirectional radiation fluxes are assumed since large variations in spacecraft attitudes tend to average out any anisotropies. However, when the spacecraft attitude is stabilized, the anisotropies in the radiation distribution can not be ignored, and a complex shielding analysis has to be performed. Such circumstances are met with the International Space Station, the attitude of which will be approximately stabilized along its velocity vector. Employing only omnidirectional model could result in errors in the shielding analysis and a hazard to the crew and electronics.

In the first part of Technical Note 6, the model of Watts et al. (1989) which combines the Heckman and Nakano (1969) pitch-angle distribution with the Lenchek and Singer (1962) East-West asymmetry factor has been reviewed and discussed. The Watts et al. model has been used by the *Science Applications International Corporation* (SAIC) to evaluated radiation shielding for manned spacecraft (Armstrong et al., 1990; Appleby et al., 1992) and to analyse data from the LDEF satellite (Armstrong et al., 1992a and 1992b). In the software tools ANISO and ANISOPOS developed in the framework of the TREND-3 study, the model of Watts et al. (1989) and an alternative version based on the Badwar and Konradi (1990) pitch-angle distribution have been implemented. The purpose of both software is to provide angular dependent proton flux spectra starting from standard omnidirectional flux NASA model AP-8. Since unidirectional trapped proton flux data bases now are available, directional models of the radiation belt can be built directly from these data bases. To this end, the trapped proton models should have the capability to incorporate

the observed unidirectional flux distributions. The purpose of this second part of Technical Note 6 is the introduction of a generalised anisotropy model for the LEO radiation environment.

The Lenchek and Singer (1962) East-West asymmetry factor, the Heckman and Nakano (1969) pitch-angle distribution, and consequently the anisotropy model of Watts et al. (1989), depend explicitely on the local value of the magnetic dip angle and of the atmospheric scale height. A trapped radiation belt model based on this type of description of the anisotropy will probably poorly satisfy the contraints imposed on the angular flux distribution by Liouville's theorem (Roederer, 1970; Hess 1968), which links the unidirectional particle fluxes observed at two different geographic position located on a same magnetic drift shell (Kruglanski and Lemaire, 1996). Such a link introduces a compulsive constraint on all model depending on local value. For the particular case of the atmospheric scale height, the problem can be bypassed by the use of an effective scale height obtained by an average over the whole drift shell and helicoidal trajectory of the protons. But this procedure cannot be generalized.

In order to obtain a more general description of the trapped proton anisotropy, we introduce an alternatieve approach to that of Watts et al. (1989). This approach is based only on the use of a coordinate system attached to the magnetic field lines. It results in a model which does not include parameters depending explicitly on the geographic location where the model is evaluated. This kind of approach is not original. It corresponds to the use of action variables, i.e. the adiabatic invariants μ, J and Φ (Schulz and Lanzerotti, 1974).

In fact, the trapped radiation models make use of coordinates stemed from the adiabatic invariants, e.g. the (E, B, L) coordinates. They are based on the common guiding centre and infinitesimal gyroradius approximations. Our approach takes into account that, when the East-West asymmetry effect is observable, it clearly invalidates the infinitesimal gyroradius approximation. Nevertheless, the guiding centre approximation generally continues to hold. The protons still have helicoidal trajectories along the magnetic field lines, bounce between their mirror points and drift around the Earth. The proposed model of the proton anisotropy continues to take advantage of this general guiding centre approximation but takes into account the finite size of the proton gyroradius.

In Chapter 4, we describe our new approach based on an extension of the usual (E, B, L) coordinate system and which allows to define a general proton East-West asymmetry model.

In Chapter 5 of this Technical Note, we confront our East-West asymmetry model to unidirectional proton flux measurements.

Chapter 4

Generalised anisotropy model

This chapter is devoted to the description of a generalised anisotropy model for the trapped proton radiation belt. The description includes the definition of magnetic drift shell parameters, a spatial natural coordinate system, and an azimuthal angle parametrising the East-West asymmetry.

4.1 Magnetic drift shell parameters

In the inner magnetosphere, trapped particles experience a cyclotron, bounce and drift motion. The cyclotron motion, which is clockwise for protons, is characterized by its Larmor radius (or gyroradius) r_{g}. The bounce motion occurs along magnetic field lines between mirror points of magnetic field intensity B_{m}. The drift motion (westwards for the protons) is perpendicular to the magnetic field lines (Roederer, 1970). Three adiabatic invariants are associated with these three different motions.

The first adiabatic invariant corresponds to the particle magnetic moment and is given by

$$\mu \equiv \frac{p_{\perp}^2}{2m_0 B} = \frac{p^2}{2m_0 B_{\mathrm{m}}}\,, \tag{4.1}$$

where $p_{\perp}$ is the component of the particle momentum $\mathbf{p}$ normal to the local magnetic field vector $\mathbf{B}$ and m_0 is the rest mass.

The second adiabatic invariant, evaluated along the bounce path, is often called the integral invariant and is given by

$$J \equiv \oint p_{\parallel} \mathrm{d}s = 2pI\,, \tag{4.2}$$

where $p_{\parallel}$ is the component of $\mathbf{p}$ parallel to $\mathbf{B}$ and s is a curvilinear coordinate that measures distance along a field line. The quantity I introduced in Eq. (4.2) has

the dimension of a length and only depends on the magnetic field configuration and on the value of B_{m}. One should note that I, called the integral invariant function, is adiabatically invariant only in a static magnetic field (in the absence of other external forces, i.e. when the particle can not be energised).

The third adiabatic invariant corresponds to the magnetic flux enclosed by the drift path of a particle. It is given by

$$\Phi \equiv q \int_S \mathbf{B} \cdot \mathrm{d}\mathbf{S}\,, \tag{4.3}$$

where q is the particle's charge and d$\mathbf{S}$ an element of a surface delimited by the drift shell, e.g. by the equatorial drift path. Equations (4.1) and (4.2) can be combined to provide a derived adiabatic invariant:

$$K \equiv \frac{J}{\sqrt{8 m_0 \mu}} = I\sqrt{B} \tag{4.4}$$

(Kaufmann, 1965) which only depends the magnetic field configuration.

The drift motion of trapped particles generates a shell encircling the Earth. The family of magnetic field line segments on which the particle guiding centre moves forms a closed surface which is identified as the magnetic drift shell of the particle. A drift shell is unequivoquely defined by the three adiabatic invariants μ, J and Φ. In the case of a strictly static magnetic field, the particle energy E is a constant of the motion and two adiabatic invariants suffice to label a magnetic drift shell. It is convenient to use the magnetic field intensity at the mirror points (B_{m}) in combination with the integral invariant function (I).

Since the quantity I is not an easy coordinate to interpret and does not vary linearly with any familiar physical quantity, McIlwain (1961) introduced a shell parameter* L, which is a function of both B_{m} and I. The function is such that, in a pure dipole magnetic field (where drift shells are axially symmetric), L is equal to the distance from the dipole centre to the equatorial crossing of the particle guiding centre. The shell parameter L is expressed in Earth radii (R_{E}). Hilton (1971) has derived a simple analytical apprximation relating L to B_{m} and I. The coordinates (B_{m}, L) fully identify a magnetic drift shell in a static magnetic field (Roederer, 1970).

*The shell parameter is sometimes noted as L_{m} to stress that the integral of Eq. (4.2) which determines I is delimited by the mirror points

4.2 Finite gyroradius effect

In the following, we consider the directional flux $f_{\mathtt{P}}(E, \alpha, \beta)$ of trapped particles of energy E observed at a point $\mathtt{P}$ in space and in the direction (α, β). The look direction is specified by spherical angles α and β relatively to a coordinate system (x, y, z): α and β correspond to the polar angle between the look direction and the z-axis, and to the azimutal angle between the projection of the look direction in the plane xy and the x-axis, respectively. In the next sections, the coordinate system will be choosen such that the z-axis corresponds to the direction of the local magnetic field vector. In our system, the directional flux $f_{\mathtt{P}}(E, \alpha, \beta)$ will then be related to particles with a velocity vector in the direction $(\pi - \alpha,\ \pi + \beta)$, i.e. with a pitch angle[†] of $\pi - \alpha$.

According to Liouville's theorem, the directional flux $f_{\mathtt{P}}(E, \alpha, \beta)$ can be converted into a function of energy and the adiabatic invariants only. When trapped particle fluxes are mapped generally with the help of the (E, B_{m}, L) coordinates,

$$f_{\mathtt{P}}(E, \alpha, \beta) = j_{\perp}(E, B_{\mathrm{m}}, L) \tag{4.5}$$

where $j_{\perp}$ is the perpendicular flux observed at the mirror points (Roederer, 1970). B_{m} and L depend both on $\mathtt{P}$, α and β. Once the relationship between the coordinates (B_{m}, L) and both location and direction of observation is established, the local particle fluxes and their anisotropies are determined everywhere in the magnetosphere.

Liouville's theorem links particle fluxes at different locations along a particle trajectory. In the infinitesimal gyroradius approximation, the helicoidal trajectory of a particle is reduced to its magnetic drift shell and the position where the particle is observed is considered to be part of its drift shell. The guiding center of the particle coincides then with the field line passing through the point of observation. This approximation is generally applied in the construction of radiation belt models. However, in regions of space where the scale length of the particle fluxes becomes of the same order of magnitude, or smaller, than r_{g}, this approximation is no longer valid. This is in particular the case for energetic trapped protons in the inner edge of the radiation belt, near the loss cone. The loss cone results from the slowing down of the trapped protons due to their interactions with the Earth's atmosphere. Its main effect on the trapped proton fluxes is the steep pitch-angle distribution observed at low altitudes (Freden and White, 1960).

For a point of observation located at the inner edge of radiation belt, the observed

[†]The pitch angle of a trapped particle is defined by the angle between the particle momentum $\mathbf{p}$ and the magnetic field vector $\mathbf{B}$. At the particle mirror points, where $B = B_{\mathrm{m}}$, the pitch angle is equal to 90°.

flux of energetic trapped protons is known to depend on the look direction, even for a fixed pitch angle (Watts et al., 1989). This effect is known as the East-West asymmetry (Heckman and Nakano, 1963). For instance, aboard the SAMPEX spacecraft, the countrate associated to 86–120 MeV protons and observed at $L \approx 1.15$ and $B_{\rm m} \approx 0.197\,$Gauss varies by a factor of 6 between the periods when the detector is looking to the East and the periods when it is looking to the West (Looper et al., 1998). This East-West effect is explained by the fact that protons viewed with the same pitch angle but in different azimuthal directions have their guiding centres on different magnetic field lines and thus belong to different drift shells, where the fluxes are rather different from each other. Consequently, to take into account that the guiding centres of the observed protons no longer correspond to the point of observation, the L value $L_{\rm GC}$ associated with the guiding centre should be used instead of the L value associated with the point of observation. This approach means that the flux maps have to be organized in (E, $B_{\rm m}$, $L_{\rm GC}$).

4.3 First order expansion of the perpendicular flux

The shell parameter $L_{\rm GC}$ associated to a guiding centre depends on the look direction and also on the particle energy through the Larmor radius

$$r_{\rm g} = \frac{p}{qB}\sin\alpha \tag{4.6}$$

where p and q are the momentum[‡] and charge of the proton, respectively, and B the local magnetic field intensity. Therefore, when building and using a model of the form $f(E, B_{\rm m}, L_{\rm GC})$, $L_{\rm GC}$ has to be evaluated for every look direction and for each energy covered by the instrument. As the computation of L involves an integration along a field line segment, building and using such models is very demanding of CPU time.

To avoid the evaluation of $L_{\rm GC}$ when using the $j_\perp(E, B_{\rm m}, L_{\rm GC})$ map, an alternative approach which uses an expansion to first order in L of the perpendicular flux is applied instead. With this approximation, Eq. (4.5) can be written as

$$\begin{aligned} f_{\rm P}(E,\alpha,\beta) &= j_\perp(E, B_{\rm m}, L_{\rm GC}) \\ &= j_\perp(E, B_{\rm m}, L) + \Delta L \times \left.\frac{\partial j_\perp}{\partial L}\right|_{E,B_{\rm m}} + O^{(2)}(\Delta L) \end{aligned} \tag{4.7}$$

[‡]The particle momentum and energy are related by $p^2c^2 = E^2 + 2m_0c^2E$ where c is the light velocity and m_0 the rest mass of the particle. For proton, $m_0 = 1.6725\ 10^{-27}$ kg.

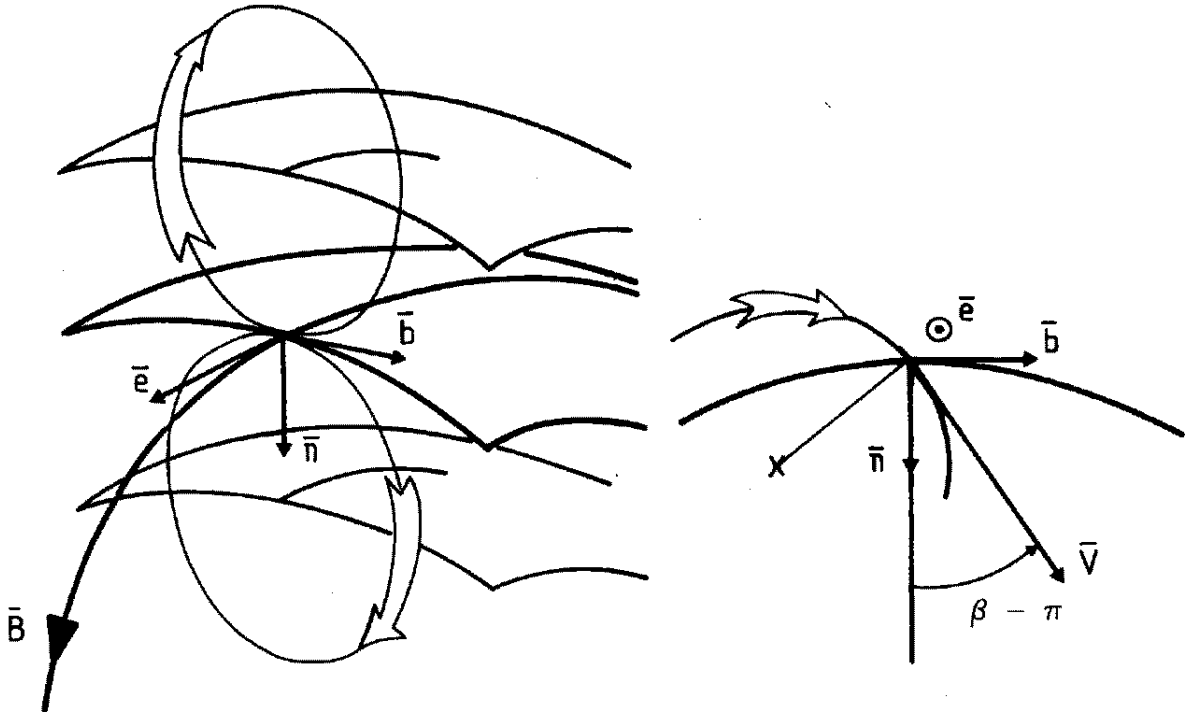

Figure 4.1. Left panel: representation of a magnetic field line segment and of three neighbouring magnetic drift shells separated by one gyroradius. The circles represent the proton gyration motions. **e**, **n** and **b** are the vectors tangent, normal and bi-normal to the magnetic field line, respectively. Right panel: Cut view in the plane $(\mathbf{n}, \mathbf{b})$ perpendicular to the magnetic field.

where $\Delta L \equiv L_{\rm GC} - L$. The $L_{\rm GC}$ evaluation problem is now reduced to evaluating ΔL, for which we propose an analytical expression in the next section. As shown below, ΔL is in close relationship with the distance between the point of observation P and the drift shell of the observed protons. For example, when P is located in the magnetic equatorial plane of a centred dipole field, ΔL is equal to the distance between the drift shell and P. The term $\partial j_\perp / \partial L$ can be computed either by direct derivation of $j_\perp$ or by comparison of experimental measurements at different ΔL.

4.4 Natural coordinate system

To evaluate $\Delta L = L_{\rm GC} - L$, we will characterize the look direction by a pair of polar and azimuthal angles (α, β) measured in a local coordinate system attached to the

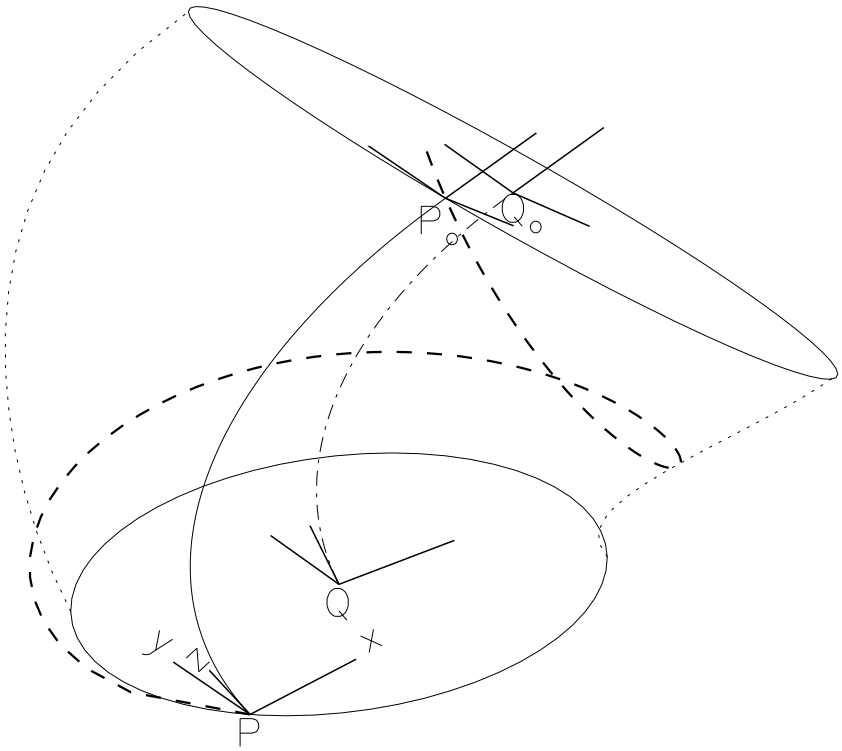

Figure 4.2. Representation of the helicoidal trajectory (dashed curve) of a particle around its guiding centre (dot-dash curve). When the particle passes through the point P ($\mathtt{P}_0$), its instantaneous guiding centre is located at Q ($\mathtt{Q}_0$, resp.). The two points P and $\mathtt{P}_0$ are located on the same magnetic field line (solid curve).

local magnetic field line. Since the drift velocity of the guiding centre of a particle is perpendicular to both the magnetic field vector $\mathbf{B}$ and the perpendicular gradient $\nabla_\perp B$ (Roederer, 1970), a natural coordinate system is such that

- the origin coincides with the point P of observation;
- the z-axis points in the direction $\mathbf{e}$ of the magnetic field vector, $\mathbf{e} = \mathbf{B}/B$;
- the x-axis points in the direction $\mathbf{n}$ of the normal to the magnetic field line, $\mathbf{n} = \nabla_\perp B/|\nabla_\perp B|$;
- the y-axis points in the direction $\mathbf{b} = \mathbf{e} \times \mathbf{n}$ of the bi-normal to the magnetic field line.

The coordinate system $(\mathbf{e}, \mathbf{n}, \mathbf{b})$ is represented in the left-hand panel of Fig. 4.1 where a magnetic field line and three neighbouring drift shells are shown. The typical

cyclotron motion of particles attached to upper and lower drift shells are displayed also. The figure illustrates that particles coming from the right do not belong to the same drift shell as particles coming from the left. If a gradient of particle flux exists, the flux of particles observed from both direction will differ. The righthand panel of Fig. 4.1 is a cut view in the plane $(\mathbf{n}, \mathbf{b})$ on which the azimuthal angle $\beta - \pi$ is defined.

In the coordinate system $(\mathbf{e}, \mathbf{n}, \mathbf{b})$, the magnetic field line and the drift shell passing through the point of observation P are parallel to the axis $\mathbf{e}$ and the plane $(\mathbf{n}, \mathbf{b})$, respectively. Consequently, when a proton is observed in the look direction (α, β), its pitch angle is equal to $\pi - \alpha$. Its gyration motion correponds to a clockwise circular motion in the plane $(\mathbf{n}, \mathbf{b})$ which is perpendicular to $\mathbf{B}$. Since the local guiding centre Q of the observed proton lies in both the plane $(\mathbf{n}, \mathbf{b})$ and the plane perpendicular to the look direction, the direction of Q is given by $(\pi/2, \beta + \pi/2)$. The distance between the local guiding centre and P is the Larmor radius $r_{\rm g}$ given by Eq. (4.6).

In the following, we will assume that $r_{\rm g}$ remains much smaller than the scale length of the magnetic field. Since the scale length of the magnetic field is about a third of the geocentric distance, this assumption remains valid in a large energy range. With this assumption, the magnetic field does not change significantly from P to Q and we can assume that the coordinate systems $(\mathbf{e}, \mathbf{n}, \mathbf{b})$ at these two locations are identical. The drift shell of a proton observed in the look direction (α, β) then contains Q and is parallel to the plane $(\mathbf{b}, \mathbf{e})$. The distance from P to the drift shell is given by

$$d_{\rm P}(\alpha, \beta) = r_g \cos(\beta + \pi/2) = -\frac{p}{qB} \sin\alpha \sin\beta \,. \tag{4.8}$$

One should note that protons viewed in the direction $(\alpha, \pi - \beta)$ will belong to the same drift shell as protons viewed in the direction (α, β) and that the proton fluxes in these two directions should be identical. In particular, when the azimuthal directions β is equal to 0 or π, the drift shell of the observed protons passes through the point of observation and $\Delta L = 0$.

4.5 Evaluation of ΔL

To establish the relationship between ΔL and the parameters such as α, β, B, L, and E, we will first connect ΔL with these parameters at the local magnetic equator[§]. Afterwards the parameters at the local magnetic equator will be connected to the same parameters at the current point of observation.

[§]In a non-dipolar magnetic field, we define the local magnetic equator as the surface where the magnetic field intensity is minimum along magnetic field lines.

Since L is defined in a centred magnetic dipole by the geocentric distance of the drift shell in the equatorial plane, we can assume that ΔL is well approximated by the distance at the magnetic equator between the drift shell of the observed proton and the drift shell passing through the point of observation, i.e.

$$\Delta L \approx -d_{\mathtt{P}_0}(\alpha_0, \beta_0) \tag{4.9}$$

where (α_0, β_0) is the look direction of protons belonging to the same drift shell as $\mathtt{Q}$ but viewed from a point $\mathtt{P}_0$ in the magnetic equatorial plane which belongs to the magnetic field line passing through $\mathtt{P}$. The minus sign takes into account that the distance to the drift shell is measured along the **n**-axis which points to decreasing L direction.

The previous statements are illustrated in Fig. 4.2 where the dashed curve represent the helicoidal trajectory of a proton passing through $\mathtt{P}$. Its guiding centre is represented by the dot-dash curve and includes the point $\mathtt{Q}$. The magnetic field line passing through $\mathtt{P}$ is represented by a solid curve. The axes of the coordinate system (**e**, **n**, **b**) are represented at both points $\mathtt{P}$ and $\mathtt{Q}$. According to the conservation of the magnetic moment, after one, two, three,... gyrations, the trajectory of the proton will cross again the magnetic field line passing through $\mathtt{P}$. So, protons belonging to the guiding centre passing through $\mathtt{Q}$ can be always observed from the equatorial point $\mathtt{P}_0$ of the magnetic field line passing through $\mathtt{P}$. For the sake of clarity, the helicoidal trajectory of Fig. 4.2 is passing through $\mathtt{P}_0$ after one gyration motion, which is generally not the case.

The protons belonging to the guiding centre passing through $\mathtt{Q}$ can be observed from both locations $\mathtt{P}$ and $\mathtt{P}_0$ but with different look directions: (α, β) and (α_0, β_0), respectively. The relationship between the polar angles α and α_0 is directly given by the conservation of the first adiabatic invariant:

$$\frac{\sin^2 \alpha_0}{B_0} = \frac{\sin^2 \alpha}{B} \tag{4.10}$$

where B_0 is the magnetic field intensity at $\mathtt{P}_0$. On the contrary, the relationship between the azimuthal angles β and β_0 is not easily established. Nevertheless, a simple relation is obtained for particular values of β:

1. When $\beta = 0$ or π, $d_{\mathtt{P}}(\alpha, \beta) = 0$, i.e. the magnetic field line passing through $\mathtt{P}$ belongs to the drift shell of the observed proton. Consequently $d_{\mathtt{P}_0}(\alpha_0, \beta_0) = 0$ and thus $\beta_0 = 0$ or π.

2. When $\beta = -\pi/2$, the drift shell of the observed proton is the most inner observable one. Since, in the magnetic equatorial plane, the drift shell shall stay the most inner one, $\beta_0 = -\pi/2$.

3. When $\beta = \pi/2$, the drift shell is the most outer observable one and $\beta_0 = \pi/2$.

For these particular cases, we simply get the relation

$$\beta_0 = \beta \,. \tag{4.11}$$

The simplicity of Equation (4.11) is due to the choice of the coordinate system, the **n**-axis of which is always perpendicular the drift shells. With regard to the other approximations made previously, we assume that the validity of Equation (4.11) can be reasonably extended to the full range of the azimuthal angles.

From Equations (4.8), (4.9), (4.10) and (4.11), the variation of the shell parameter with the azimuthal angle β is approximately given by

$$\begin{aligned} \Delta L &= r_{\mathrm{g}0} \sin\beta \\ &= \frac{p}{q\sqrt{B_0 B_{\mathrm{m}}}} \sin\beta \,. \end{aligned} \tag{4.12}$$

The magnetic field intensities B_0 and B_{m} are related to the local values by the relations

$$\left\{ \begin{array}{rcl} B_{\mathrm{m}} &=& \dfrac{B}{\sin^2\alpha} \\ \\ B_0 &=& \dfrac{M}{L^3} \end{array} \right. \tag{4.13}$$

where the magnetic moment M is arbitrary set to the same value used to compute the parameter L (McIlwain, 1961), i.e. $0.311653\,\mathrm{Gauss}\,R_{\mathrm{E}}^{-3}$. When combined to Eq. (4.7), Eq. (4.12) provides a description of the unidirectional proton fluxes which includes the East-West asymmetry.

4.6 Comments

In such a way, Eqs. (4.7) and (4.12) provide a complete description of the trapped proton fluxes at any location in the whole magnetosphere. Equation (4.7) can be re-written to highlight the main parameters:

$$f_{\mathrm{P}}(\alpha,\beta) = j_\perp(E, B_{\mathrm{m}}, L) + \left[\frac{\sqrt{E^2 + 2m_0c^2E}}{qc \quad \sqrt{M B_{\mathrm{m}} L^{-3}}}\right] \sin\beta \times \left.\frac{\partial j_\perp}{\partial L}\right|_{E,B_{\mathrm{m}}} \tag{4.14}$$

From Eq. (4.14), it appears clearly that the observed flux $f_{\mathrm{P}}(\alpha,\beta)$ is only a function of E, B_{m}, L and β where the perpendicular flux $j_\perp(E, B_{\mathrm{m}}, L)$ and $\partial j_\perp/\partial L$ have to

be determined from unidirectional measurements. As a default, the NASA unidirectional model UP-8 can be used. On should note that the perpendicular flux model depends only on the particle energy E and drift shell labels (B_m, L).

As stressed in the first part of Technical Note 6 (Kruglanski and Lemaire, 1996), the constraint on $f_\mathtt{P}$ resulting from the application of Liouville's theorem can be written as

$$\int_0^{2\pi} \frac{f_\mathtt{P}(\alpha,\beta)}{E}\,\mathrm{d}\beta = \int_0^{2\pi} \frac{f'_\mathtt{P}(\alpha',\beta)}{E}\,\mathrm{d}\beta \tag{4.15}$$

where the both points $\mathtt{P}$ and $\mathtt{P}'$ are located on the same drift shell (i.e. $B_\mathrm{m} = B'_\mathrm{m}$ and $L = L'$) and where the pitch angles α and α' are related by the conservation of μ. In the case of the flux function of Eq. (4.14), the equality of Eq. (4.15) is always true. Equation (4.14) complies with Liouville's theorem.

The trapped proton East-West asymmetry effect is usually linked to atmospheric scale height (Lenchek and Singer, 1962; Watts et al., 1989). In our aproach, no atmospheric parameter appears in Eq. (4.14). In fact the effect of the atmosphere is already present in the model of the perpendicular flux $j_\perp$. Nevertheless, it would be nice if an effective scale height could be deduce from Eq. (4.14). To this end, we introduce a flux scale height defined by

$$H_{j\perp} \equiv \frac{j_\perp}{\left.\dfrac{\partial j_\perp}{\partial L}\right|_{E,B_\mathrm{m}}} \tag{4.16}$$

Note that there is no minus sign present in the definition such that the scale height is positive when the flux $j_\perp$ increases with L.

As a first order approximation, it can be easily shown that Eq. (4.14) is equivalent to

$$f_\mathtt{P}(\alpha,\beta) = j_\perp(E,B_\mathrm{m},L)\exp\left(\frac{\sin\beta\, r_\mathrm{gm}}{H_{j\perp}}\sqrt{\frac{B_\mathrm{m}}{ML^{-3}}}\right) \tag{4.17}$$

where r_gm is the Larmor radius at the mirror point of the particles. An East-West asymmetry factor can be deduced from Eq. (4.17) by comparing the flux of particles from the local magnetic West ($\beta = \pi/2$) to the flux of particles coming from the local magnetic East ($\beta = -\pi/2$):

$$\frac{f_\mathtt{P}(\alpha,\pi/2)}{f_\mathtt{P}(\alpha,-\pi/2)} = \exp\left(\frac{2r_\mathrm{gm}}{H_{j\perp}}/\sin\alpha_0\right) \tag{4.18}$$

One should be aware that Eqs. (4.17) and (4.18) have been established for small value of the exponential argument.

Chapter 5

Comparison with observational data

Equations (4.7) and (4.12) of the Chapter 4 provide a new semi-empirical model for the description of the trapped proton anisotropy at low altitudes. In this model the dependence of the particle flux on the azimuthal angle β is based on theoretical assumptions while the dependence on the pitch angle α has to be obtained empirically from a data set of measurements.

This new semi-empirical model has to be confronted with measurements of directional proton flux in the radiation belts. Note that the model also needs data for the values of $j_\perp$ and $\partial j_\perp / \partial L$. Three datasets of unidirectional proton fluxes in the SAA have been studied in TREND-3:

- AZUR/EI-88 with a field of view of $\pm 21°$;
- SAMPEX/PET with a field of view of $\pm 30°$;
- UARS/HEPS with a field of view of $\pm 15°$.

A detailed description of these satellite missions and their instruments can be found in Technical Note 5 part I, II and III, respectively. Unfortunately, up to now, only the PET data can be used to test and evaluate the new model, since

- a lack in the AZUR documentation prevents the computation of the azimuthal angle from the ephemeris data;
- the 3-axis stabilised attitude of the UARS spacecraft reduces the variation of β to a very small angle range for a fixed value of B_m and L.

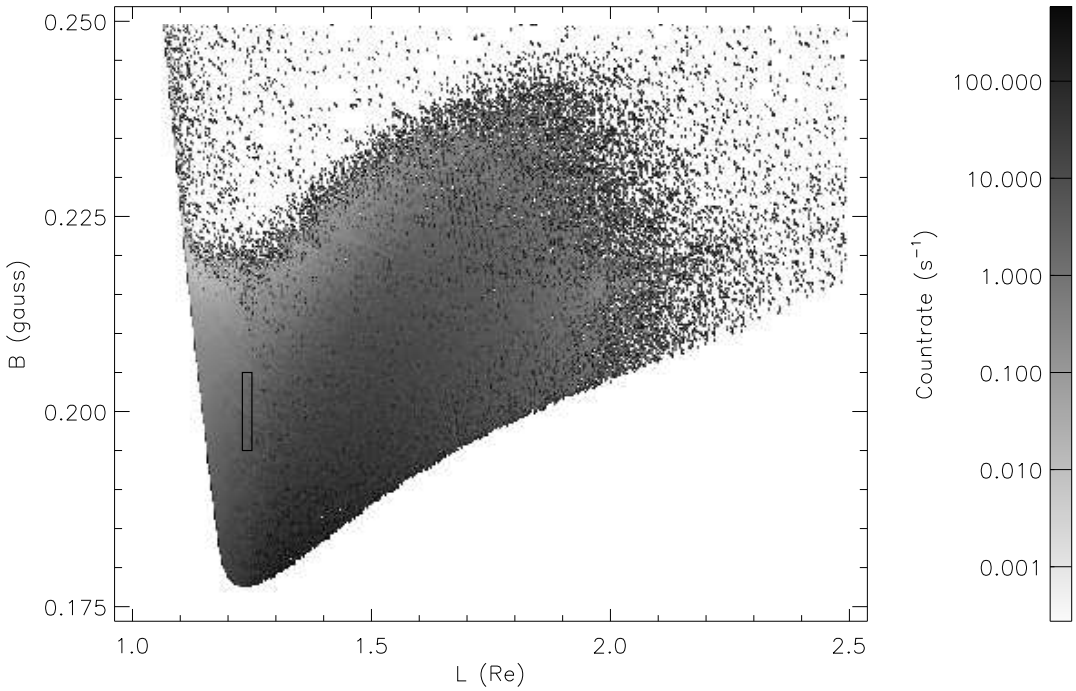

Figure 5.1. (B, L) diagram of the SAMPEX 86–120 MeV proton countrate. The rectangular box corresponds to the bin selected to test the new semi-empirical model.

To test the new semi-empirical model, we have selected from the SAMPEX/PET data a bin in $(E, B_{\rm m}, L)$ space for the period of time which extends from mid 1994 to mid 1995. The bin is specified by

$$\begin{aligned} 0.195 < B_{\rm m} < 0.205\,, \\ 1.23 < L < 1.25\,, \\ 86.1 < E < 120.0\,. \end{aligned} \tag{5.1}$$

The IGRF 1995 magnetic field model is used to evaluate the $B_{\rm m}$ and L values. The energy range corresponds to the channel `pen/p81` of the PET instrument. The Larmor radius at the mirror point corresponding to the central point of the bin specified by Eqs. (5.1) is equal to 77.2 km. It varies from `???` to `???` km inside te bin. The bin is represented on Fig. 5.1 where the countrates of the channel `pen/p81` are shown as function of $B_{\rm m}$ and L.

The magnetic drift shell ($L = 1.24$, $B_{\rm m} = 0.2$) which corresponds to the central point of the selected SAMPEX data bin, is represented in a 3-D view in Fig. 5.2.

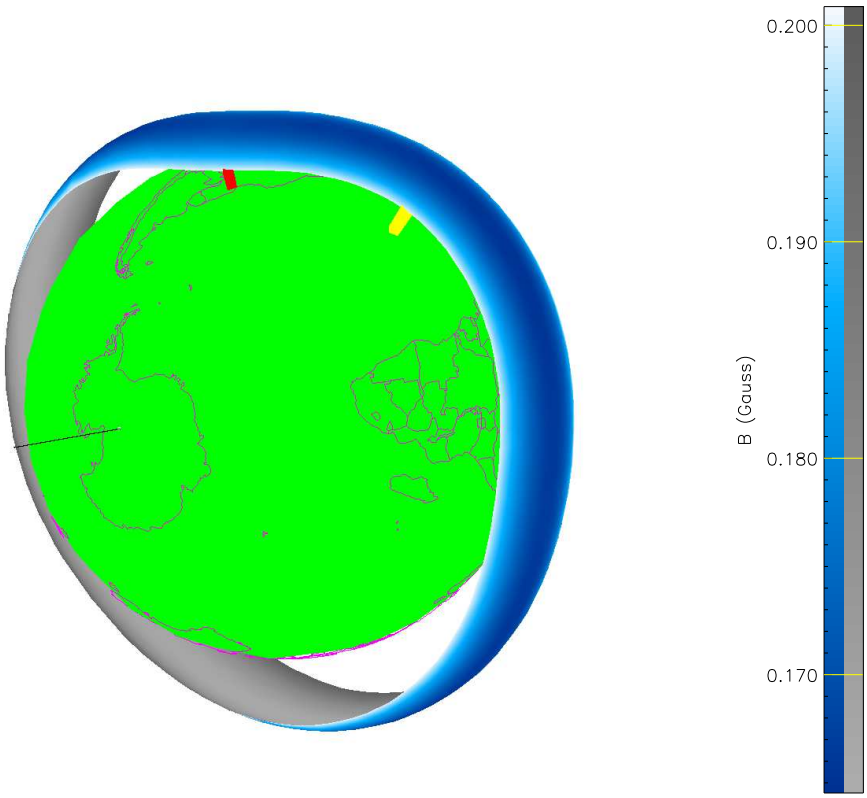

Figure 5.2. Representation of the magnetic drift shell $L = 1.24$, $B_{\mathrm{m}} = 0.2$. The two bars correspond to two mirror points in the southern hemisphere with a longitude of 51°W and 15°W, respectively. The IGRF 1995 magnetic field model has been used to trace the drift shell.

The drift shell is clearly not axially symmetric and is mainly deformed near the SAA region. The altitudes of the southern mirror points are shown on Fig. 5.3 as a function of the mirror point longitude. The lowest altitude on the shell is located at the mirror point 394.3 km, 25.7°S and 51.0°W. The location of this particular mirror point is indicated by a dotted line in Fig. 5.3 and by a dark bar in Fig. 5.2.

In Sect. 5.4, the new semi-empirical model is compared to two other models for two mirror points on the drift shell: the point of lowest altitude, and a second one located at 720.8 km, 7.9°S and 15.0°W (The second mirror point is highlighted on Figs. 5.2 and 5.3).

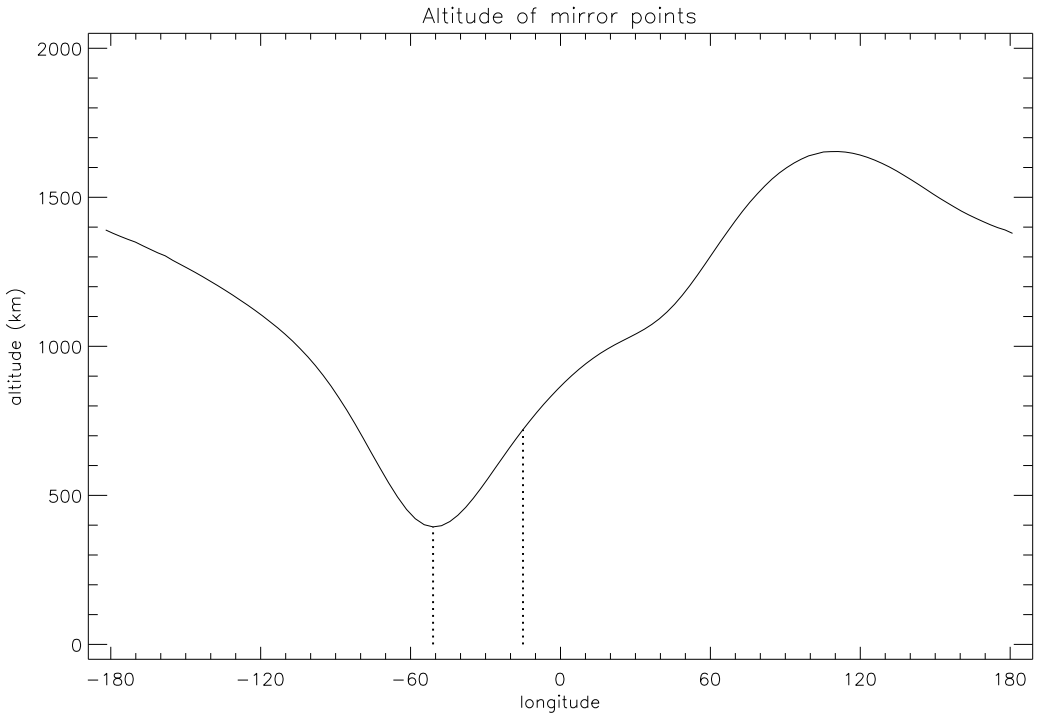

Figure 5.3. Geocentric altitude of the southern mirror points of the drift shell ($L = 1.24$, $B_{\rm m} = 0.2$) as a function of the mirror point longitude. The dotted lines indicate the mirror point with the lowest altitude (at 51°W of longitude) and an other mirror point located at 336.5 km higher (at 15°W of longitude).

5.1 Variation of $L_{\rm GC}$

Equation (4.12) predicts a variation of the shell parameter with respect to the azimuthal parameter given by

$$\Delta L = r_{\rm gm} \sqrt{\frac{B_{\rm m}}{B_0}} \sin \beta \tag{5.2}$$

where $r_{\rm gm}$ and $B_{\rm m}$ are the gyroradius and magnetic field intensity at the mirror point. The validity of Eq. (4.12) or (5.2) depends only on the configuration of the magnetic field model. Instead of selecting, at random, geographic positions and look directions to evaluate the validity of these equations, we have used the SAMPEX ephemeris as a test case for the assumptions and approximations underlying Eq. (5.2).

For each point of the ephemeris in the bin defined by Eqs. (5.1), we have evaluated the shell parameter L as well as the value $L_{\rm GC}$ of the shell parameter at the guiding

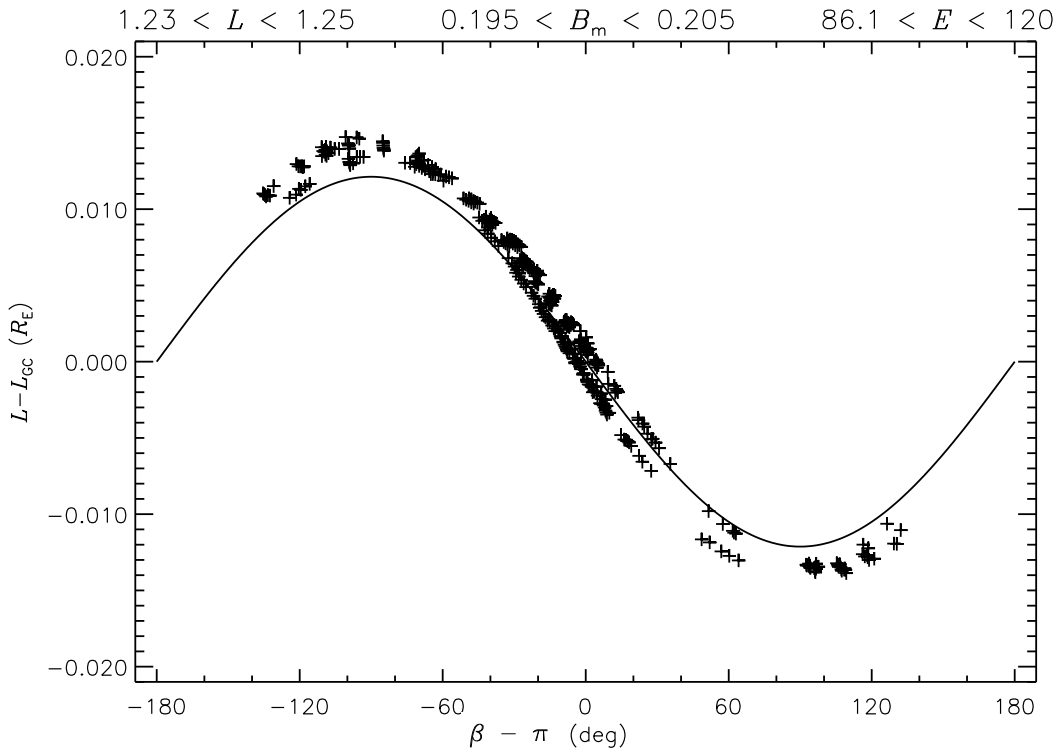

Figure 5.4. The variation ΔL of the shell parameter obtained in Eq. (4.12) as a function of the azimuthal angle β (solid curve) is compared to the difference $L - L_{\rm GC}$ obtained from the SAMPEX ephemeris (+ symbols) in the coordinate bin defined in the text.

centre of 100 MeV protons. In Fig. 5.4, the difference $L - L_{\rm GC}$ is compared to the sinusoidal variation ΔL predicted by Eq. (4.12) for $B_{\rm m} = 0.20$ and $L = 1.24$. The relatively good agreement between ΔL and the ephemeris data validates the approximation done in the determination of ΔL. The residual scattering of the ephemeris data is attributed to the range of $B_{\rm m}$ and L in the bin. There is a small acceptable disagreement around $\beta = \pm\pi/2$.

5.2 Flux scale height

To apply the new semi-empirical model, the profile of the perpendicular flux with respect to L first has to be determined. This profile will provide the two undetermined parameters of Eq. (4.7): $j_\perp$ and its derivative with respect to L.

The profile of the perpendicular flux as a function of the shell parameter L has been obtained by selecting the PET data for which $-0.05 < \sin\beta < 0.05$,

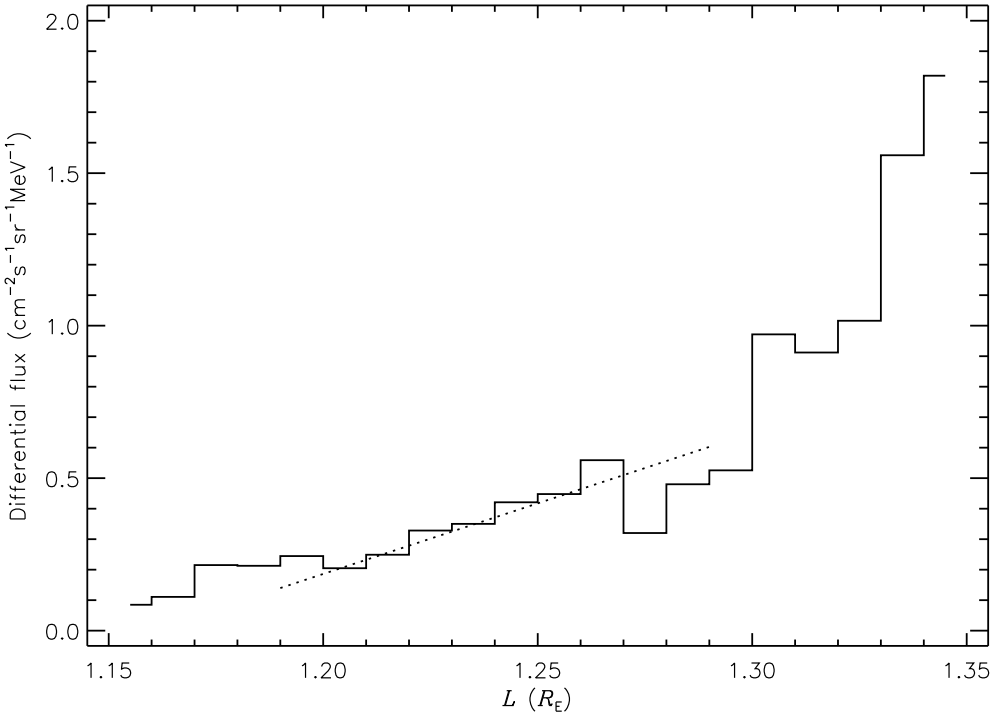

Figure 5.5. Dependence of the SAMPEX 86–120 MeV proton countrate on L for $0.195 < B_m < 0.205$ and $|\sin\beta| < 0.05$. The dotted curve corresponds to a linear fit based on the data for which $1.23 < L < 1.25$.

$0.195 < B_m < 0.205$ and $1.15 < L < 1.35$. The selection on $\sin\beta$ filters those measurements with L_{GC} values close to L, so that $j_\perp$ is well approximated by the mean of the selected fluxes, and that a linear fit can be used to determine $\partial j_\perp/\partial L$. Figure 5.5 shows the dependence on L of the proton countrate of the data points that meet the above conditions. Note that individual points are not represented on the figure due to the small livetime of the measurements. In Fig. 5.5, the data points have been binned in twenty L bins between $L = 1.15$ and 1.35. The problem relative to small livetime is specific to the PET data and is fully discussed in Technical Note 5, Part II.

Figure 5.6 shows a "zoom" of Fig. 5.5 around $L = 1.24$. The data points have again been binned in twenty L bins between $L = 1.23$ and 1.25. A linear fit of the binned flux of Fig. 5.6 is used to evaluate the flux at $L = 1.24$ and the value of its derivative. The linear fit is given by

$$j_\perp = 0.375\,\mathrm{cm^{-2}s^{-1}sr^{-1}MeV^{-1}}, \qquad \frac{\partial j_\perp}{\partial L} = 4.63\,\mathrm{cm^{-2}s^{-1}sr^{-1}MeV^{-1}}R_E^{-1}\,. \quad (5.3)$$

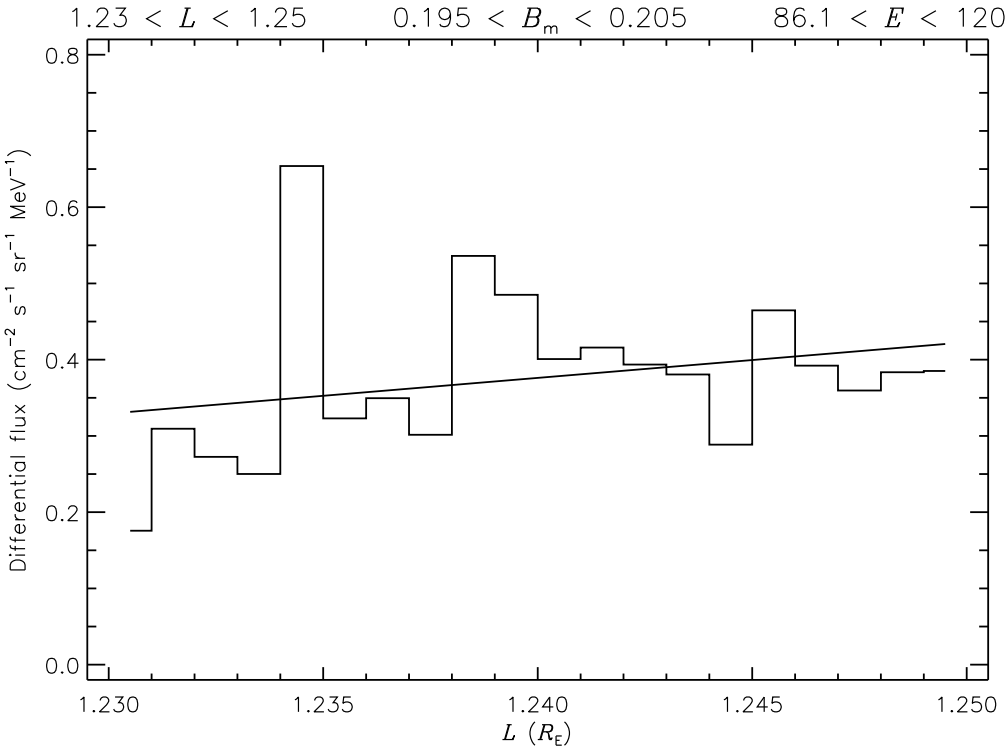

Figure 5.6. Dependence of the SAMPEX 86–120 MeV proton countrate on L for $0.195 < B_{\rm m} < 0.205$, $1.23 < L < 1.25$ and $|\sin\beta| < 0.05$. The solid line corresponds to a linear fit.

The linear fit is represented on Figs. 5.5 and 5.6 by a dotted line and a solid line, respectively. One should note the large scattering of the binned data around the linear fit. The scattering is related to the Poisson statistic behaviour of the PET measurements. Unfortunately this behaviour complicates the evaluation of the new semi-empirical model.

5.3 East-West asymmetry

For the bin defined by Eqs. (5.1), we have evaluated the dependence of the observed flux on the azimuthal angle β. In Fig. 5.7, the flux obtained with Eq. (4.7) is compared to the SAMPEX/PET measurements in the selected bin. As before, the data points have been binned, now in twenty β bins. Note that the bins around $\beta = 0^\circ$ are empty.

Now that the dependence on L of the perpendicular flux is determined, Eq. (4.7) can be used to evaluate the East-West asymmetry effect. The East-West effect

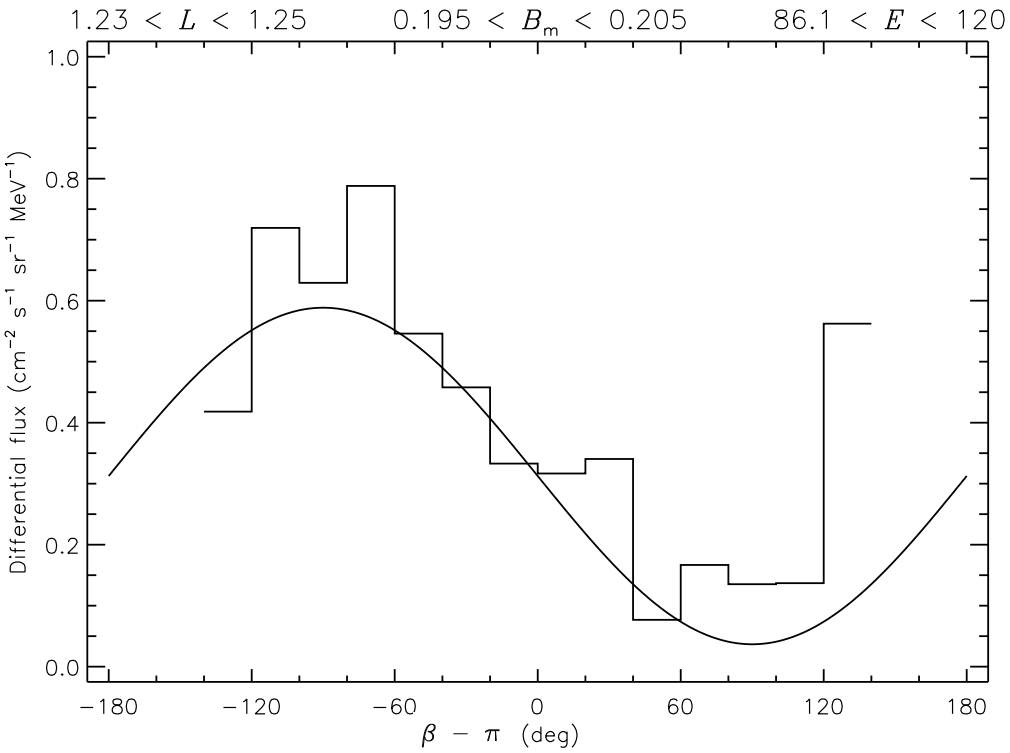

Figure 5.7. Dependence on the SAMPEX 86–120 MeV proton countrate as a function of the azimuthal angle β for the points in the bin ($0.195 < B_{\rm m} < 0.205$, $1.23 < L < 1.25$), i.e. the same points as Fig. 5.4. The solid curve corresponds to the linear fit of Fig. 5.6 where ΔL is obtained from Equation (4.12).

predicted by the new semi-empirical model is a sine curve, which is represented in Fig. 5.7 as a solid line. The main trend of the binned data is well rendered by the sine curve. Nevertheless the scatter around the sine curve is large. Part of the scattering is due to the finite size of the bin in both B, L and energy. Further uncertainties are introduced by the relatively large opening angle (60°)of the PET instrument which creates an uncertainty on the angles α and β. Finally, the saturation problem of the PET (see TN5), resulting in low proton count rates, adds an inherent uncertainty factor. The combined data scatter prohibits a quantitative assessment of the model. Therefore, comparisons of the model to the directional dependence of PET data in other bins will probably not improve the validation. Morever, even with one year of data, the coverage in β is not complete in all (B, L) bins.

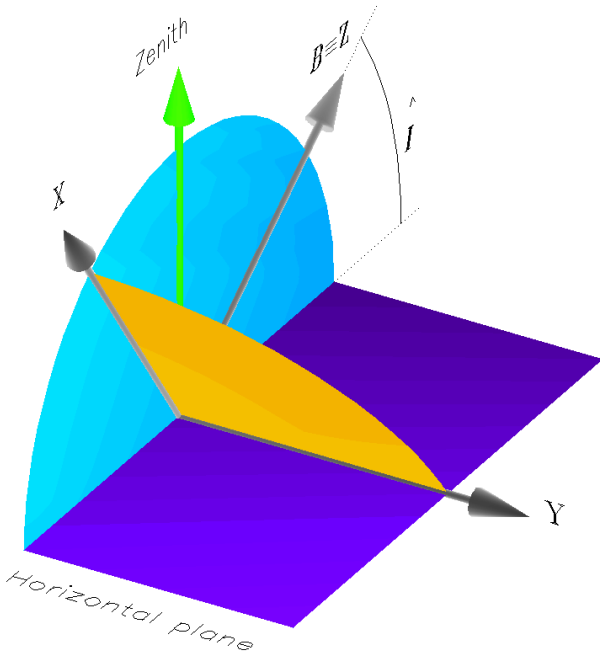

Figure 5.8. Representation of the coordinate system used to compare different proton anisotropy models

5.4 Comparison with previous models

In this section, we compare the new semi-empirical model to two other models: the model of Watts et al. (1989) and the BK-MIN model developed early. Since both models has been already discussed in Part I of this technical note (Kruglanski and Lemaire, 1996), they are only briefly reviewed. For the sake of clarity, the omnidirectional fluxes of both models are normalized to unity, and the look directions are determined in a coordinate system such that

1. the Z-axis is parallel to the magnetic field vector;
2. the Y-axis lies in the local horizontal plane and points in the magnetic East direction;
3. the plane XZ contains the zenith direction, i.e. it is a local vertical plane;
4. the plane XY corresponds to the local mirror plane.

The coordinate system is represented in a 3-D view on Fig. 5.8. The representation in Fig. 5.8 includes the local horizontal plane, the local mirror plane and the local vertical plane which contains the magnetic field vector. Note that the coordinate system (Z, X, Y) differs from the coordinate system (**e**, **n**, **b**) [defined in Sect. 4.4]

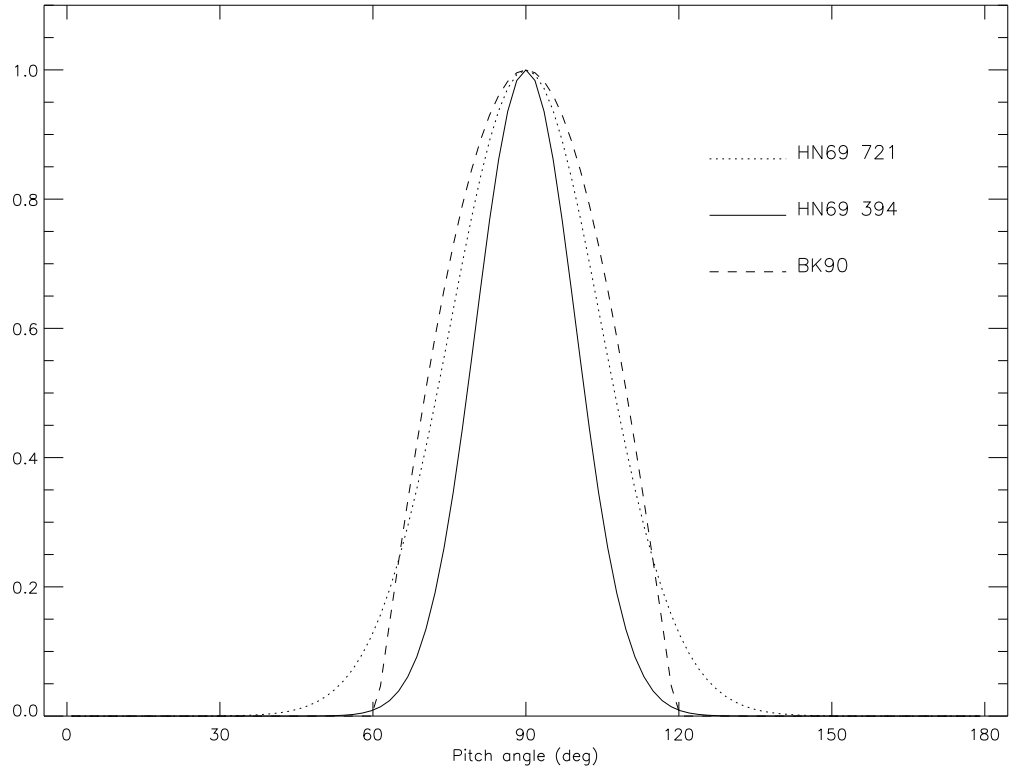

Figure 5.9. Comparison of the Heckman & Nakano (1969) and Badhwar & Konradi (1990) pitch angle distributions at $L = 1.24$ and $B_{\rm m} = 0.2$. The dotted and solid lines correspond to the Heckman & Nakano (1969) distribution evaluated at an altitude of 720.8 and 394.3 km, respectively. The dashed line corresponds to the Badhwar & Konradi (1990) distribution, whatever the altitude. Note that the normalisation is such that $f(\pi/2) = 1$.

by a rotation about the Z-axis only, i.e. the azimuthal angle ϕ differs from the angle β by an offset. The value of this offset depends on the magnetic field configuration, and thus on the geographic position.

The model of Watts et al. (1989) use the Heckman & Nakano (1969) pitch-angle distribution. This distribution is given by

$$f_{\rm HN}(\alpha) = \frac{\exp\left(-\dfrac{(\pi/2-\alpha)^2}{2\sigma^2}\right)}{\sigma\sqrt{2\pi}\,\mathrm{erf}\left(\dfrac{\pi}{\sigma\sqrt{8}}\right)} \tag{5.4}$$

where the square of the standard deviation is

$$\sigma^2 = \frac{3}{4}\frac{H}{R}(2 + \cos^2 \hat{I}) \,, \tag{5.5}$$

H is the atmospheric scale height, R the distance from the Earth's centre, and $\hat{I}$ the magnetic dip angle, i.e. the angle between the magnetic field vector and the local horizontal plane. For convenience, the angle $\hat{I}$ is represented also on Fig. 5.8

The BK-MIN model uses the Badhwar & Konradi (1990) pitch-angle distribution which is given by

$$f_{\rm BK}(\alpha) = \begin{cases} \xi \exp(-b\xi) & \alpha_{0c} < \alpha_0 < \pi - \alpha_{0c} \\ 0 & \text{otherwise} \end{cases} \tag{5.6}$$

where

$$\xi = \frac{\sin\alpha_0 - \sin\alpha_{0c}}{\sqrt{B_0}} \,, \tag{5.7}$$

b and α_{0c} are two parameters determined empirically. Note that the $f_{\rm BK}$ pitch-angle distribution does not depend on local variable (such as $\hat{I}$) but depends insteads on the shell parameter L and particle energy E.

The Lenchek and Singer (1962) asymmetry function is used by both the Watts et al. (1989) and the BK-MIN models. It is given by

$$g_{\rm LS}(\alpha, \phi) = \frac{\exp(r_{\rm g} \cos\hat{I} \sin\phi / H)}{2\pi \mathrm{I}_0(r_{\rm g} \cos\hat{I}/H)} \tag{5.8}$$

where the azimuthal angle ϕ measures, in the local mirror plane, the deviation from the X-axis. Note that the $g_{\rm LS}$ function depends on the pitch angle through the expression of the gyroradius [see Eq. (4.6)]. The azimuthal angle ϕ is much convenient to be evaluated than angle β but it has too a less physical meaning than angle β.

5.4.1 Watts et al. (1989) model

The model developed by Watts et al. (1989) combines the the pitch angle distribution proposed by Heckman and Nakano (1969) and the finite gyroradius effect described by Lencheck and Singer (1962). The conversion factor to transform omnidirectional flux into directional flux is given by

$$W_{\rm HN-LS}(\alpha, \phi) = \frac{f_{\rm HN}(\alpha) g_{\rm LS}(\phi)}{\sin\alpha} \tag{5.9}$$

where the atmospheric scale height for solar minimum is given by

$$H = 33.4\,\mathrm{km} \times \exp\left(\frac{R - 6371.2\,\mathrm{km}}{383\,\mathrm{km}}\right) \tag{5.10}$$

(Colborn et al., 1990). At 394.3 and 720.8 km altitude, the atmospheric scale height of Eq. (5.10) is equal to 93.5 and 219.3 km, respectively.

5.4.2 BK-MIN model

For the empirical BK-MIN model based on the pitch angle distribution of Badhwar and Konradi (1989), the conversion factor* from omnidirectional fluxes to unidirectional fluxes is given by

$$W_{\mathrm{BK-LS}}(\alpha, \phi) = \frac{f_{\mathrm{BK}}(\alpha) g_{\mathrm{LS}}(\phi)}{\int_0^\pi \sin\alpha' f_{\mathrm{BK}}(\alpha') \mathrm{d}\alpha'}\,. \tag{5.11}$$

For the purpose of the comparison, the parameters b and $\alpha_{0\mathrm{c}}$ of the Badhwar & Konradi (1990) function have been fitted on the SAMPEX countrates presented on Fig. 5.6. To facilitate the inter-comparison, the atmospheric scale height appearing in function g_{LS} is evaluated using Eq. (5.10) also instead of a fixed value. Note that contrary to the Watts et al. (1989) model, the function $W_{\mathrm{BK-LS}}$ satisfies Eq. (4.15), i.e. Liouville's theorem averaged over the azimutal angle ϕ.

5.4.3 New semi-empirical model

The new semi-empirical model is obtained by implementing Eq. (4.14) where the pitch angle distribution of the perpendicular flux is described with the Badhwar and Konradi distribution:

$$j_\perp(E, B_{\mathrm{m}}, L) = K f_{\mathrm{BK}}(\alpha) \tag{5.12}$$

where K is a scaling parameter to be fit on the data in the same way as the parameters $\alpha_{0\mathrm{c}}$ and b. The conversion factor from omnidirectional fluxes to unidirectional fluxes is then given by

$$W_{\mathrm{BK-beta}}(\alpha, \phi) = \frac{f_{\mathtt{P}}[\alpha, \beta(\phi)]}{\iint f_{\mathtt{P}}(\alpha, \beta) \sin\alpha\, \mathrm{d}\alpha\, \mathrm{d}\beta}\,. \tag{5.13}$$

*One should note that a separate normalisation is applied in Eq. (5.11) instead of a global normalisation, as described in Part I of the Technical Note

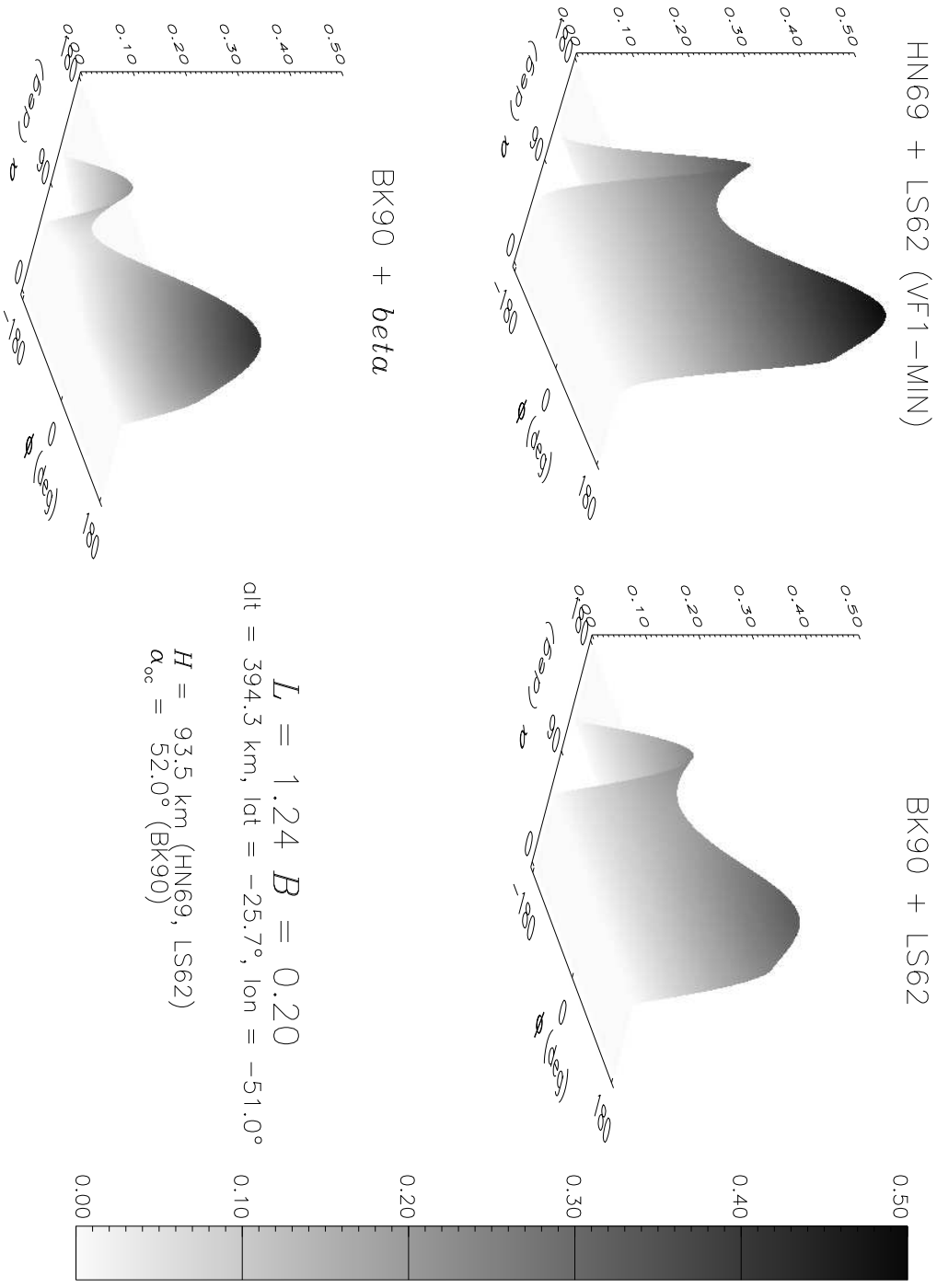

Figure 5.10. Dependence of the directional 100-MeV proton flux on the polar and azimuthal direction at the position (394.3 km, 25.7°S, 51.0°W)

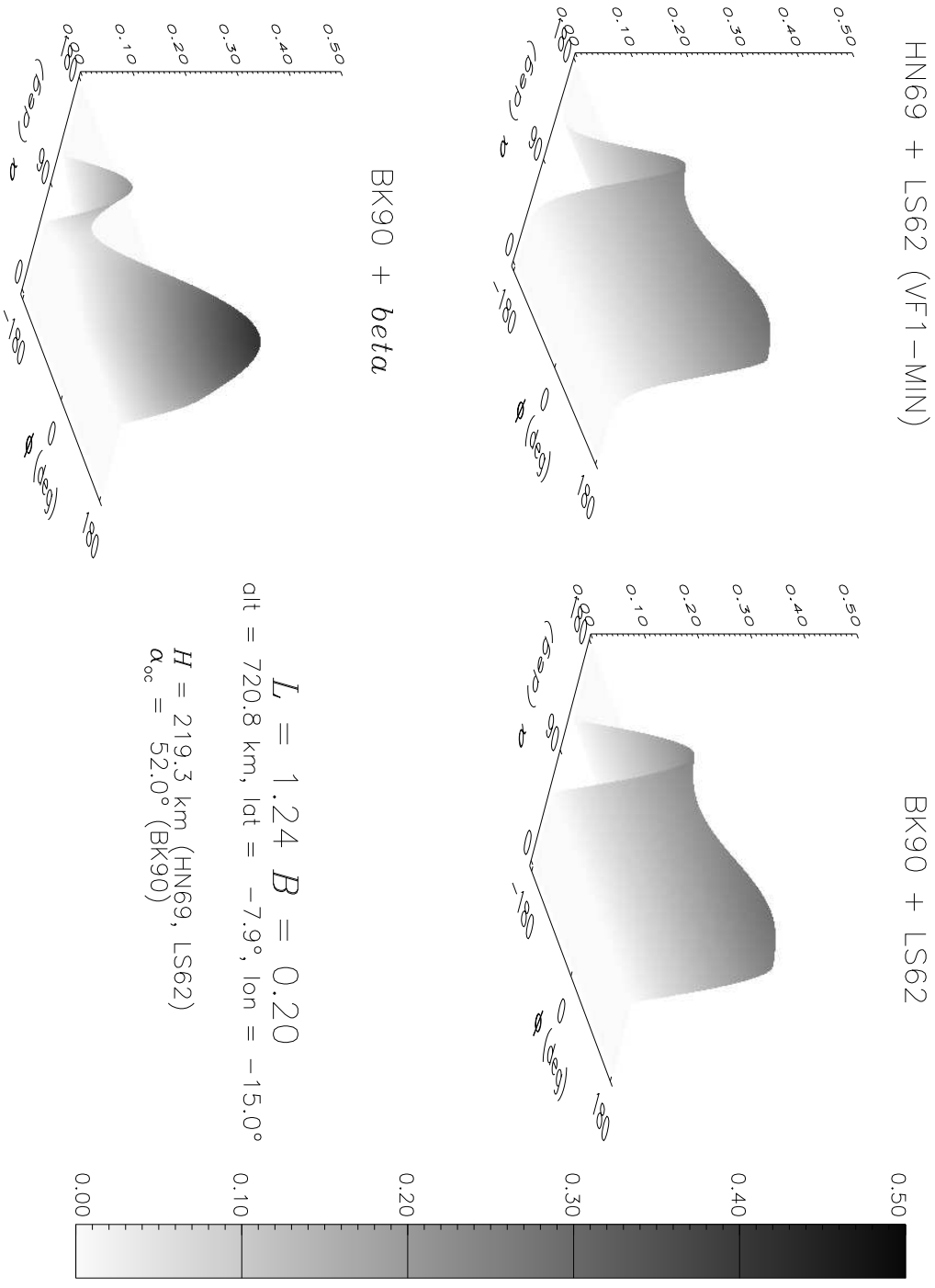

Figure 5.11. Dependence of the directional 100-MeV proton flux on the polar and azimuthal direction at the position (720.8 km, 7.9°S, 15.0°W)

The functions $W_{\mathrm{BK-LS}}$ and $W_{\mathrm{BK-beta}}$ satisfy Eq. (4.15). The function $W_{\mathrm{BK-beta}}$ has the advantage to be built in a more consistent way without depending on the atmospheric parameter H.

5.4.4 Comparison

In Fig. 5.9, the pitch-angle distributions f_{HN} and f_{BK} are compared at two geographic locations: (394.3 km, 25.7°S, 51.0°W) and (720.8 km, 7.9°S, 15.0°W), i.e. the two mirror points on the drift shell defined at the start of this chapter and highlighted on Figs. 5.2 and 5.3. Since the Badhwar & Konradi (1990) function depends only on E and L, the f_{BK} pitch-angle distribution is identical at both locations. On the other hand, the variation of the ratio H/R from 1/72 to 1/32 between the two locations implies an important change of the Heckman & Nakano (1969) pitch-angle distribution. As mentioned (Sect. 4.6) already, a varying pitch-angle distribution is not compatible with Liouville's theorem which imposes a single pitch angle distribution for all mirror points on a given drift shell (B, L). Therefore, models based on the f_{HN} function have to be restricted to a region of space where the ratio H/R does not vary.

The conversion factors, $W_{\mathrm{HN-LS}}$, $W_{\mathrm{BK-LS}}$ and $W_{\mathrm{BK-beta}}$, of the three defined models, are compared at the two different geographic locations selected from the set of mirror points of the magnetic drift shell $L = 1.24$, $B_{\mathrm{m}} = 0.2$, shown in Fig. 5.2. As mentioned before, the two selected mirror points are located at (394.3 km, 25.7°S, 51.0°W) and (720.8 km, 7.9°S, 15.0°W), respectively.

In Figs. 5.10 and 5.11, the dependences of the flux on the polar and azimuthal angles (α, ϕ) predicted by both models are compared at the two geographic locations for 100 MeV protons. Only the conversion factors $W_{\mathrm{HN-LS}}$, $W_{\mathrm{BK-LS}}$ and $W_{\mathrm{BK-beta}}$ are represented on both figures. In Fig. 5.10, which corresponds to the lowest mirror point, the East-West asymmetry is apparent for the three models. One should note that the new semi-empirical model is more asymmetric than the two others.

In Fig. 5.11, the asymmetry is much reduced for the $W_{\mathrm{HN-LS}}$ and $W_{\mathrm{BK-LS}}$ functions. This reduction is due to the variation by a factor 7/3 of the atmospheric scale height between 394 and 721 km of altitude. On the other hand, the asymmetry of the new semi-empirical model remains unchanged. Between Fig. 5.10 and Fig. 5.11, the function $W_{\mathrm{BK-beta}}$ has not changed except by a small shift in the azimuthal angle due to a variation of the offset between the angles β and ϕ.

References

Appleby, M.H., Griffin B.N., Turner E.R., Pogue, W.R., Golightly M.J.: 1992, *Computer Aided Radiation Analysis for Manned Spacecraft*, Proc. 22nd International Conference on Environmental Systems, Seattle, WA, July 13–16

Armstrong, T.W., Colborn, B.L., Watts, J.W.: 1990, *Characteristics of Trapped Proton Anisotropy at Space Station Freedom Altitudes*, Science Applications International Corporation Report SAIC-90/1474

Armstrong, T.W., Colborn, B.L., Watts, J.W.: 1992a, *Ionizing Radiation Calculations and Comparisons With LDEF Data*, First LDEF Post-Retrieval Symposium, NASA-CP-3134

Armstrong, T.W., Colborn, B.L., Harmon, B.A., Parnell, T.A., Watts, J.W., Jr., Benton, E.V.: 1992b *Comparison of Model Predictions With LDEF Satellite Radiation Measurements*, World Space Congress, 29th Plenary Meeting of COSPAR, Washington D.C., August 29–September 5, Paper F2.7-M.1.06X

Badhwar, G.D., Konradi, A.: 1990, *Conversion of Omnidirectional Proton Fluxes Into a Pitch-angle Distribution*, J. Spacecraft and Rockets **27**, 350

Colborn, B.L., Watts, J.W., Armstrong, T.W.: 1990 *Data Base Description and Retrieval Program for the Trapped Proton Vector Flux Data Bases VF1MAX and VF1MIN*, Science Applications International Corporation Report SAIC-90/1475

Freden, S.C., White, R.S.: 1960, *Particle Fluxes in the Inner Radiation Belt*, J. Geophys. Res. **65**, 1377–1383

Heckman, H.H., Nakano, G.H.: 1963, *East-West Asymmetry in the Flux of Mirroring Geomagnetically Trapped Protons*, J. Geophys. Res. **68**, 2117–2120

Heckman, H.H., Nakano, G.H.: 1969, *Low-Altitude Trapped Protons during Solar Minimum Period*, 1962-1966, J. Geophys. Res. **74**, 3575–3590

Hess, W.N.: 1968, *The Radiation Belt and Magnetosphere*, Blaisdell Publishing Company, Waltham (Massachusetts)

Heynderickx, D., Kruglanski, M.: 1997, *Flight Data Comparisons*, Technical Note **5**, ESTEC/ESA, contract no 10725/94/NL/JG(SC)

Hilton, H.H.: 1971, *L Parameter, A New Approximation*, J. Geophys. Res. **76**,

6952–6954

Kaufmann, R.L.: 1965, *Conservation of the First and Second Adiabatic Invariants*, J. Geophys. Res. **70**, 2181–2186

Kruglanski, M., Lemaire, J.: 1996, *Trapped Proton Anisotropy at Low-Altitudes*, Technical Note **6**, ESTEC/ESA, contract no 10725/94/NL/JG(SC)

Lenchek, A.M., Singer, S.F.: 1962, *Effects of the Finite Gyroradii of Geomagnetically Trapped Protons*, J. Geophys. Res. **67**, 4073–4075

Looper, M.D., Blake, J.B., Mewaldt, R.A.: 1998, *Maps of Hydrogen Isotopes at Low-Altitude in the Inner Zone from SAMPEX Observations*, Adv. Sp. Res., in press

McIlwain, C.E.: 1961, *Coordinates for Mapping the Distribution of Magnetically Trapped Particles*, J. Geophys. Res. **66**, 3681–3691

Roederer, J.G.: 1970, *Dynamics of Geomagnetically Trapped Radiation*, Springer-Verlag, Berlin

Schulz, M., Lanzerotti, L.J.: 1974, *Particle Diffusion in Radiation Belts*, Springer-Verlag, New York

Watts, J.W., Parnell, T.A., Heckman, H.H.: 1989, *Approximate Angular Distribution and Spectra for Geomagnetically Trapped Protons in Low-Earth Orbit*, Conf. on High-Energy Radiation in Background Space, A.C. Rester Jr. and J.I. Trombka (Eds.), Santibel Island, FL 1987, Am. Inst. Phys. Conf. Proc., New York, 75–85